Optical-Model Analysis of 50- and 64-MeV Alpha-Particle Scattering from ^{58}Ni and ^{58}Fe†

David C. Weisser,* J. S. Lilley, Russell K. Hobbie, and G. W. Greenlees
John H. Williams Laboratory of Nuclear Physics, University of Minnesota, Minneapolis, Minnesota 55455
(Received 6 April 1970)

An optical-model analysis of the scattering of 64.3-MeV α particles from ^{58}Ni and ^{58}Fe, and of 50.2-MeV α particles from ^{58}Ni, has been performed using independent real- and imaginary-potential-geometry parameters. The scattering is found to be sensitive only to the potential form at radial distances beyond about 6 F. Real-potential-parameter ambiguities have been studied with particular reference to the quality of the analyzed data. The potentials found are compared with expectations based upon a simple folding of matter sizes and effective two-body forces.

I. INTRODUCTION

Recently, relatively detailed studies[1-3] have been made of the representation of the elastic scattering of nucleons by an optical model. These studies have emphasized that only limited information concerning the potential can be extracted from such analyses and have gone some way towards relating such potentials to nuclear neutron and proton distributions and nucleon-nucleon forces. The present paper attempts a similar approach, using α-particle elastic-scattering data. Among the complex particles, the α particle is the most appropriate for such investigations, since its relatively high-binding energy makes it reasonable to neglect the excitation of the projectile, which would greatly complicate interpretation of the results. If such an assumption is justified, α elastic-scattering potentials represent a simplification over the proton case, since no spin-orbit interaction is involved. The purpose of the present work, therefore, is to determine to what extent information concerning the potential and nuclear sizes can be obtained from optical-model analyses of α-particle scattering data.

Previous optical-model analyses of α-particle scattering data have given real-potential radii significantly larger than the corresponding quantities determined from proton data. Schemes that account for this difference by adding to the proton potential radius a constant term for the finite size of the α particle have had limited success.[4-6] In order to minimize the number of parameters, analyses have tended to use the same geometry for the real and imaginary potentials. In general, the data analyzed are such that little improvement in the quality of fitting is achieved if the geometries are uncoupled, and the increased number of parameters cannot be justified. It is unlikely that the two geometries are the same, and the values found, presumably, represent some kind of average between the optimum real and imaginary forms. This indicates a need for more accurate and extensive α-particle elastic-scattering data. Where independent real and imaginary geometries have been used to analyze relatively extensive data,[7] the imaginary-potential radius is found to be larger than that of the real potential.

The present work attempts to explore the parameter space of the α-nucleus elastic-scattering potential in some detail using independent real- and imaginary-potential geometries. The parameter ambiguities are examined, and also the relationship of the potentials to the corresponding proton potentials and nuclear-matter distributions.

II. α-PARTICLE POTENTIALS

In an optical-model analysis the elastic scattering is represented by the scattering of a point particle by a spherically symmetric potential. In the present case, this potential has the form

$$V(r) = V_{\mathrm{Coul}} - V_{\mathrm{R}}\, f(r) - iW_{\mathrm{V}} g(r) + iW_{\mathrm{D}}\, 4a_{\mathrm{I}}\, g'(r), \tag{1}$$

where V_{Coul} is the Coulomb potential

$$f(r) = \{1 + e^{(r - r_{\mathrm{R}} A^{1/3})/a_{\mathrm{R}}}\}^{-1},$$

and

$$g(r) = \{1 + e^{(r - r_{\mathrm{I}} A^{1/3})/a_{\mathrm{I}}}\}^{-1}.$$

The fact that α particles are strongly absorbed in nuclear matter results in the scattering being dominated by the potential at large radii and being insensitive to the interior form. This emphasis on the potential surface has been expressed by Igo[5] by

the relation

$$C_1 = V_R^i \, e^{R_R^i / a_R^i}, \tag{2}$$

where i corresponds to the ith real potential that fits the data;

$$R_R^i = r_R^i A^{1/3};$$

and C_1 is a constant for all i.

Although Eq. (2) is consistent with a continuum of values of V_R, only discrete sets of parameters are found to be compatible with the data. This discreteness is attributed to integral numbers of nodes of the wave function inside the potential.[8] In general, acceptable real-potential parameters give values of C_1 which, although not constant, have relatively small variation. It is to be expected that a relationship similar to Eq. (2) will hold for the imaginary-potential parameters, when these have independent geometry. However, the evidence is less satisfactory than in the case of the real potential.[6-8] It has been suggested[9] that the magnitudes of the potentials at the strong absorption radius constitute a more satisfactory criterion than Eq. (2).

If the use of independent real and imaginary geometries is to be justified, it is necessary that the experimental data be both accurate and detailed. This point has been examined by Broek *et al.*[7] for the scattering of 43-MeV α particles by ^{58}Ni. They found that with errors of less than 2%, an angular range covering five relatively deep cross-section minima was needed to specify the imaginary potential unambiguously.

The angular distributions chosen for the present investigation were available in numerical form at 50.2 MeV[10] from ^{58}Ni and at 64.3 MeV[11] from ^{58}Ni and ^{58}Fe. These data satisfied the criteria established by Broek *et al.* Most attention was paid to the data from ^{58}Ni at 64.3 MeV. This angular distribution contains significant structure and has been measured with good accuracy; errors are less than 1% at forward angles and about 2–3% at backward angles (Fig. 1). Reference 11 also provided data of comparable quality for ^{58}Fe at 64.3 MeV (Fig. 2). The data at 50.2 MeV for ^{58}Ni (Fig. 3) contained several pronounced oscillations in the angular distribution, with errors of ±5%. Some data at 21.08 MeV[12] were also studied, although these did not satisfy the strict criteria for accuracy and detail discussed above.

III. ANALYSIS

The optical-model potential used in this analysis is given by Eq. (1) with the Coulomb potential taken to be that of a Woods-Saxon charge distribution of

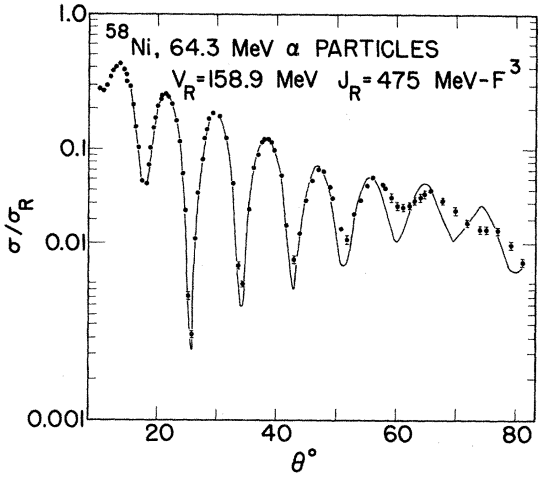

FIG. 1. A typical fit to 64.3-MeV α-particle elastic scattering data from ^{58}Ni (Ref. 11) for one of the equivalent potentials of Table I.

diffuseness 0.502 F and radius $(1.106 + 1.053 \times 10^{-4} A) A^{1/3}$ F.[1,13] The computer code RAROMP[13] was used. The goodness of fit was measured by the usual χ^2 criterion where

$$\chi^2 = \frac{1}{N} \sum_{i=1}^{N} \left[\frac{\sigma_{th}(\theta_i) - \sigma_{exp}(\theta_i)}{\Delta \sigma_{exp}(\theta_i)} \right]^2$$

and $\sigma_{th}(\theta_i)$, $\sigma_{exp}(\theta_i)$, and $\Delta\sigma_{exp}(\theta_i)$ are the predicted cross section, the measured cross section, and the error in the measured cross section, respectively, at angle θ_i, and N is the number of data points. The search routine varied parameters to find a minimum in χ^2.

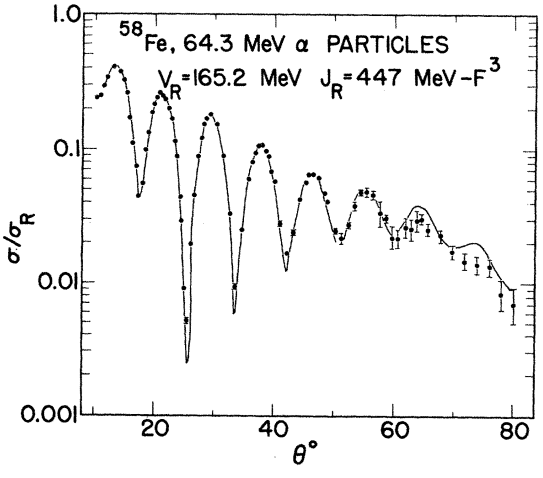

FIG. 2. A typical fit to 64.3-MeV α-particle elastic scattering data from ^{58}Fe (Ref. 11) for one of the equivalent potentials of Table II.

A. ^{58}Ni at 64.3 MeV

For the ^{58}Ni data at 64.3 MeV, preliminary explorations of the parameter space were started near $V_R = 200$ MeV with a volume form for both the real and imaginary potentials. Well-known characteristics of optical-model analyses for strongly absorbed particles were found: There was a preference for r_I to be larger than r_R and for a_I to be smaller than a_R.[7] Equally good fits to the data were obtained using either a surface or a volume imaginary potential, or a combination of the two. These alternative imaginary potentials were almost identical for radial distances greater than 6.5 F but significantly different for smaller distances. This facet of the analysis is discussed later.

The real-potential ambiguities were investigated by fixing r_R at a succession of values and varying all other parameters for a best fit. Using small values for r_R yielded large values for V_R and vice versa. However, the correlation was not continuous in V_R, which changed in multiples of about 50 MeV from approximately 150 MeV with r_R around 1.35 F to 300 MeV with r_R around 1.2 F. Accompanying these changes in V_R were changes of about 100 MeV F^3 in the volume integral per particle pair of the real potential, J_R ($=J/4A$), where A is the mass number of the target, and J is the volume integral of the nuclear potential given by

$$J = V_R\, 4\pi \int_0^\infty r^2 f(r)\,dr$$

$$= V_R\, \tfrac{4}{3}\pi R_R^3 \left[1 + (\pi a_R)^2/R_R^2\right] \qquad (3)$$

for the potential of Eq. (1).

Recent analyses of elastic proton scattering[1-3] have shown that the volume integral of the real central optical-model potential is well defined for acceptable fits to the data, whereas the individual strength and geometrical parameters can vary within wide limits. The quality of fit in these analyses appeared to be sensitive to the volume integral of the real potential and not to its detailed shape. This suggested that in the present case, it might be more appropriate to characterize the alternate families of real-potential parameters fitting the data by their volume integrals, as defined by Eq. (3), rather than by their depths. This approach, using volume integrals, proved to be more satisfactory than the depths in separating different families, and was used in the present analysis.

In an analysis of the present type, the χ^2 minimum found in the parameter space can be prejudiced by the starting values chosen. An attempt was made to avoid these difficulties by using the following procedure. The starting values for the imaginary-potential parameters were $W_D = 0$, W_V

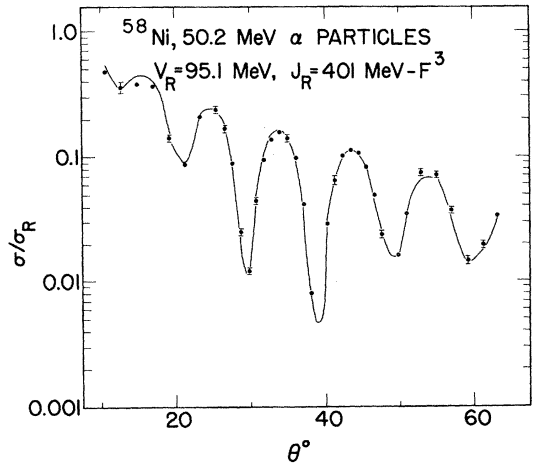

FIG. 3. A typical fit to 50.2-MeV α-particle elastic scattering data from ^{58}Ni (Ref. 10) for one of the equivalent potentials of Table III.

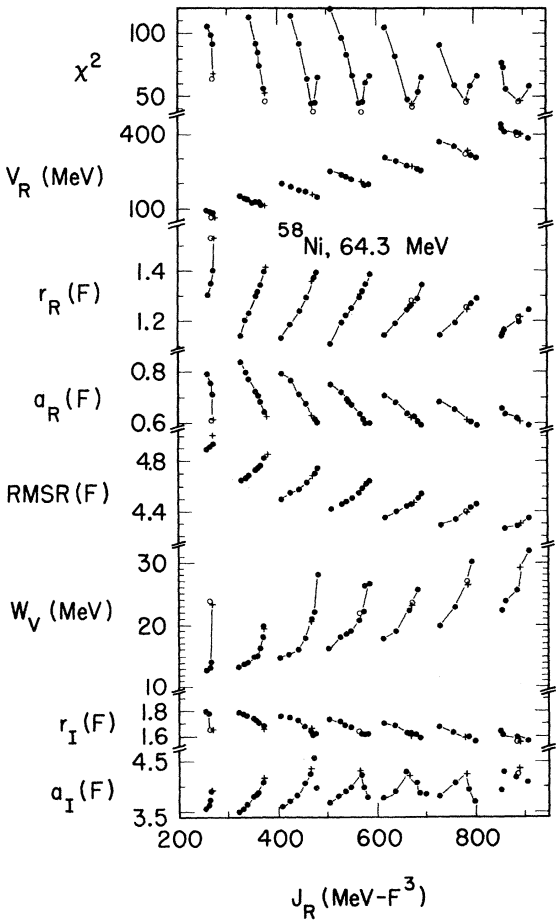

FIG. 4. Parameter correlations and the corresponding χ^2 values found for the 64.3-MeV data from ^{58}Ni, obtained as described in the text. Several equivalent minima in χ^2 are seen.

= 20 MeV, $r_I = 1.5$ F, and $a_I = 0.4$ F. The real radius parameter r_R, was then fixed at values between 1.15 and 1.40 F in steps of 0.05 F. For each r_R value, the starting value of a_R was taken to be 0.65 F, and the starting value of V_R varied from 25 to 300 MeV in 25-MeV steps, and from 350 to 600 MeV in 50-MeV steps. For each initial combination a minimum in χ^2 was found by searching on V_R, a_R, W_V, r_I, and a_I (W_D was taken to be zero). In some cases values of r_R greater than 1.4 F were investigated. A summary of the results of these searches is presented in Fig. 4. This figure shows a series of well-defined minima in χ^2 as a function of J_R, and systematic changes of the other parameters as variations away from the minima are effected. The parameters giving the lowest χ^2 in the grids on r_R were used as starting values for the final fits, which were obtained from a search varying all parameters including r_R. This produced negligible changes in the parameters. The values obtained for each family are given in Table I, and a plot of the predictions for the family with $J_R = 475$ MeV F^3 is included in Fig. 1. Investigations were also made beyond the range shown in Fig. 4 (i.e., where V_R <100 MeV or >400 MeV) but these always produced χ^2 values at least 1.5 times greater than the best shown in Fig. 4 and are not included.

B. ^{58}Fe at 64.3 MeV

The above investigation of the 64.3-MeV α-particle scattering from ^{58}Ni was used as a guide to extend this type of analysis to other cases. The time-consuming mapping of the families of parameters for each discrete potential was not repeated. In the case of ^{58}Fe at 64.3 MeV,[11] the family with $V_R \sim 200$ MeV ($J_R \sim 580$ MeV F^3) was examined using an r_R grid as described above, and found to be similar to the ^{58}Ni case. These results, together with the systematics found in Sec. III A, were used to choose starting parameters for a search for the best-fit parameters for the other families. The parameters for the equivalent potentials are given in Table II, and a plot of the predictions for the family with $J_R \sim 447$ MeV F^3 is included in Fig. 2.

C. ^{58}Ni at 50.2 MeV

A similar analysis was performed for the 50.2-MeV α-particle data from ^{58}Ni of Ref. 10. This resulted in the parameters listed in Table III, and a plot of the predictions for the family with $J_R \sim 401$ MeV F^3 is included in Fig. 3. Since this angular distribution contained only about half the number of oscillations of the one at 64.3 MeV, and the experimental errors were two to five times greater, the χ^2 minima were much broader. This was evidenced by the increased width of the χ^2 versus J_R minima.

The correlation between the accuracy of the data analyzed and the acceptable range of parameter values for a given family was investigated to some extent using the ^{58}Ni data at 64.3 MeV.[11] The

TABLE I. ^{58}Ni, 64.3 MeV, equivalent potentials.

V_R (MeV)	r_R (F)	a_R (F)	rmsr (F)	W_V (MeV)	r_I (F)	a_I (F)	J_R (MeV F^3)	χ^2	$10^{-5}C_1$	$10^{-7}C_2$	σ_R (mb)
111.4	1.423	0.625	4.857	20.0	1.661	0.420	379	47	7.5	8.85	1591
158.9	1.357	0.629	4.693	21.0	1.641	0.438	475	38	6.8	4.15	1592
209.4	1.316	0.625	4.579	22.3	1.631	0.437	575	39	7.2	4.17	1590
266.4	1.281	0.622	4.483	24.1	1.621	0.433	677	41	7.8	4.71	1588
326.1	1.258	0.615	4.410	27.4	1.607	0.429	787	46	9.0	5.40	1587
397.3	1.226	0.615	4.327	29.7	1.594	0.430	893	47	9.9	5.04	1585

TABLE II. ^{58}Fe, 64.3 MeV, equivalent potentials.

V_R (MeV)	r_R (F)	a_R (F)	rmsr (F)	W_V (MeV)	r_I (F)	a_I (F)	J_R (MeV F^3)	χ^2	$10^{-5}C_1$	$10^{-7}C_2$	σ_R (mb)
36.7	1.589	0.635	5.315	23.3	1.586	0.598	170	18	5.8	6.67	1698
78.5	1.438	0.663	4.964	24.1	1.576	0.579	279	17	3.5	9.04	1681
118.1	1.356	0.676	4.779	23.6	1.581	0.571	359	17	2.8	10.6	1677
165.2	1.300	0.670	4.625	25.2	1.546	0.601	447	15	3.0	5.30	1684
220.4	1.250	0.670	4.499	26.7	1.537	0.598	536	15	3.0	5.57	1683
283.4	1.206	0.672	4.393	27.9	1.544	0.578	627	16	3.0	8.60	1676
352.8	1.170	0.671	4.303	29.4	1.548	0.561	721	17	3.0	12.7	1671
430.0	1.147	0.658	4.219	32.8	1.498	0.599	827	15	3.6	5.23	1686

TABLE III. ^{58}Ni, 50.2 MeV, equivalent potentials.

V_R (MeV)	r_R (F)	a_R (F)	rmsr (F)	W_V (MeV)	r_I (F)	a_I (F)	J_R (MeV F^3)	χ^2	$10^{-6}C_1$	$10^{-12}C_2$
57.2	1.652	0.487	5.272	18.6	1.717	0.221	285	11	28.2	211.0
95.1	1.555	0.516	5.040	19.6	1.692	0.246	402	10	10.6	7.0
132.9	1.505	0.518	4.905	20.8	1.678	0.250	511	10	9.9	4.0
178.4	1.450	0.540	4.787	20.7	1.687	0.251	621	12	5.8	4.1
225.6	1.424	0.531	4.703	25.3	1.671	0.253	745	12	7.4	3.2
269.0	1.394	0.533	4.624	26.0	1.655	0.259	836	12	6.8	1.4
327.3	1.366	0.530	4.544	27.7	1.634	0.272	961	11	7.0	0.3

original analysis of these data was presented in Sec. III A. These data were randomized to be consistent with 5% errors and then reanalyzed over the minimum around $J_R = 550$ MeV F^3 ($V_R \sim 200$ MeV). The process was then repeated using 10% errors. The widths of the χ^2-J_R minima at $\chi^2 = 1.5\ \chi^2_{min}$ for the original data (1–3%), the 5% data, and the 10% data were 24, 34, and 50 MeV F^3, respectively. For the restricted angular range at 50.2 MeV with 5% data, the corresponding width was about 100 MeV F^3. Since the minima are only separated by about 100 MeV F^3, it is clear that data containing structure comparable with that at 64.3 MeV (Fig. 1) and an accuracy of better than 5% are needed if well-separated families are to be obtained using uncoupled real and imaginary geometries. In the case of some 21.08-MeV data for ^{58}Ni,[12] it proved not to be possible to separate the parameter families using independent real and imaginary geometries.

IV. RESULTS

The discrete equivalent real potentials for the ^{58}Ni data at 64.3 MeV (Table I) are plotted in Fig. 5. The potentials are closely similar for all $r > 7$ F. A similar situation holds for the ^{58}Fe data at 64.3 MeV and the ^{58}Ni data at 50.2 MeV. This feature is represented by the constancy of C_1 in the Igo criterion of Eq. (2). Values obtained for C_1 in the three cases examined are included in the corresponding Tables (I, II, and III). With the exception of the first family in Table III, the values listed are constant within a factor 1.5. The quantity C_1 is extremely sensitive to the diffuseness parameter a_R, and a large fraction of the variation seen is due to minor variations in a_R. If the strength of the potential in the surface region is well determined, as is apparent from Fig. 5, then constancy of C_1 implies constancy of a_R. Since, in these calculations, the imaginary geometry is independent-

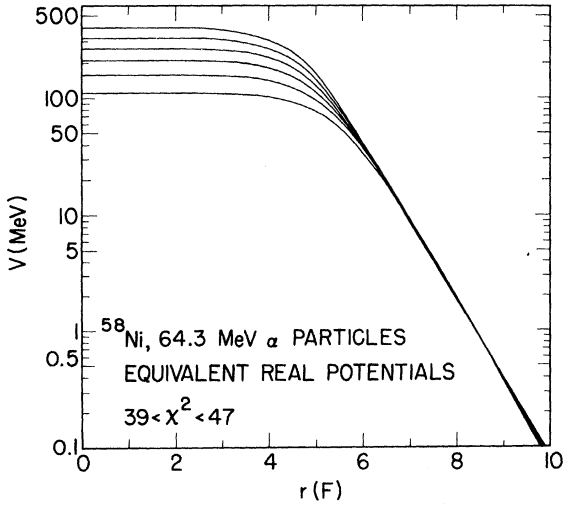

FIG. 5. Plots of equivalent real potentials for the 64.3-MeV data from ^{58}Ni. The potentials are similar for large r values.

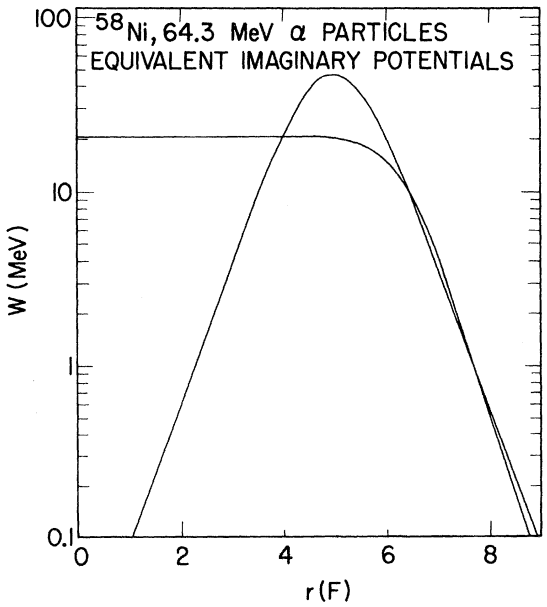

FIG. 6. Plots of the optimum imaginary potentials using volume and surface forms. In both cases the real potential parameters were $V_R = 159.8$ MeV, $r_R = 1.354$ F, and $a_R = 0.632$ F. For the volume form, $W_V = 20.8$ MeV, $r_I = 1.645$ F, $a_I = 0.437$ F, and $\chi^2 = 42$. For the surface form $W_D = 47.2$ MeV, $r_I = 1.278$ F, $a_I = 0.517$ F, and $\chi^2 = 55$. The potentials are similar for large r values.

ly variable, it is perhaps not surprising that the best set of parameters for any given family shows some variation from the mean in the C_1 values. Keeping a_R constant for all families would only marginally worsen the fits with an improvement in the agreement of C_1 values.

A similar situation applies to the imaginary potentials found here; equivalent fits to the data are obtained with either a surface or a volume shape so long as these have the same form at large distances. This is illustrated in Fig. 6 for ^{58}Ni. The values for the imaginary potential C_2, defined by Eq. (2), are included in the tables. The constancy of C_2 for the results at 64.3 MeV is comparable to that of C_1. However, at 50.2 MeV a wide spread in C_2 is observed (factor of 20) which can be attributed to the less comprehensive nature of the experimental data.

As mentioned previously, the ^{58}Ni data[12] at 21.08 MeV did not yield distinct families of parameters when an independent imaginary geometry was used. It is interesting to note, however, that the original analysis[12] of these data yields C_1 values for alternative parameter sets which agree within a factor of 2, but the corresponding C_2 values vary by 11 orders of magnitude. This suggests that, whereas limited α-particle elastic-scattering data give reasonable values for the tail of the real part of the optical-model potential, relatively detailed and extensive data are needed to define the corresponding imaginary potential.

V. DISCUSSION

The minimum χ^2 values of the various families shown in Fig. 4 differ by less than a factor of 2 and offer no basis on which to choose an optimum parameter set. This choice is usually made by analogy with the potentials found in analyses of nucleon-nucleus scattering data. Recent analyses of such data[1-3] have shown that the well-defined quantities determined by the data are the volume integral ($4AJ_R$) and the root-mean-square radius (rmsr) of the real central potential. Inspection of Tables I, II, and III, where these quantities are listed, shows clearly that a similar situation does not hold in the α-particle case, where only the tail of the potential is important. It is nevertheless interesting to see if any of the parameter families of the present analysis correspond to expectations based on analysis of nucleon-nucleus data.

An analysis of nucleon-nucleus elastic-scattering data has been made recently[1] using a model which is readily extended to cover the α-particle case. In that work the real parts (direct central, isospin central, and spin orbit) of the nucleon-nucleus potential are obtained from a folding of the nuclear-matter distribution with specific components of the nucleon-nucleon force. In the case of α-particle elastic scattering an additional folding of the matter distribution of the α particle is required, together with the assumption that no excitation of the α particle takes place during the interaction. This leads to the relationships

$$\langle r^2\rangle_R = \langle r^2\rangle_m + \langle r^2\rangle_d + \langle r^2\rangle_\alpha ,$$

and

$$J = 4A\,J_d ,$$

where $\langle r^2\rangle$ is the mean-square radius of the real potential (R), the nuclear-matter distribution (m), the direct part of the nucleon-nucleon force (d), and the α particle (α), J_d is the volume integral of the direct part of the nucleon-nucleon force, and J is the volume integral of the real potential. To a good approximation the folding procedure produces a potential of shape similar to a Woods-Saxon form with the same half-way radius as the matter distribution, but with a larger diffuseness. Taking the values for J_d and $\langle r^2\rangle_m$ found in the proton analyses[1] leads to the following expectations for α scattering for mass number 58: (1) $J_R \sim 400$ MeV F^3; (2) $V_R \sim 180$ MeV; (3) $\langle r^2\rangle_R^{1/2} \sim 4.7$ F; and (4) $r_R \sim 1.15$ F, $a_R \sim 0.85$ F. A comparison of these values with those in Tables I, II, and III shows that for the 64.3-MeV data there is fair agreement with one of the acceptable parameter families for expectations (1), (2), and (3), but disagreement with (4). At 50.2 MeV no significant agreement is evident. The phenomenological potentials for α particles clearly need a half-way radius significantly larger than the corresponding nuclear-matter radius for the best fit. This disagreement with expectations of the model of Ref. 1 for the α-particle data is perhaps not surprising. In this case only the tail of the potential is playing a role in determining the scattering, and the shape of the tail will be more dependent on the detailed functional forms used than on gross features such as the volume integral and the mean-square radius.

A similar approach to that of Ref. 1 has been applied to the analysis of α-particle data by Jackson and Kembhavi.[14] These authors combined the nucleon-nucleon force and the α-particle matter distribution and parametrized it as a Yukawa form. This Yukawa was then folded with the nuclear-matter distribution. The gross features of elastic angular distributions were reproduced, but no detailed fitting of the type presented here was attempted.

In conclusion, the elastic scattering of α parti-

cles by ^{58}Ni and ^{58}Fe can be well represented by an optical model, but only the potential at distances greater than about 6–7 F is well determined. The real potential in this region can be obtained from relatively inextensive measurements, but to determine the imaginary-potential tail requires accurate measurements over a wide angular region showing considerable structure. It is unlikely that such data will yield useful information concerning nuclear sizes, but the possibility of obtaining information concerning nuclear densities at large radii cannot be excluded.

---

†Work supported in part by the U. S. Atomic Energy Commission. This is AEC Report No. COO-1265-85.

*Present address: Physics Department, California Institute of Technology, California.

[1]G. W. Greenlees, G. J. Pyle, and Y. C. Tang, Phys. Rev. 171, 1115 (1968).

[2]G. W. Greenlees, W. Makofske, and G. J. Pyle, Phys. Rev. C 1, 1145 (1970).

[3]F. D. Becchetti, Jr., and G. W. Greenlees, Phys. Rev. 182, 1190 (1969).

[4]L. McFadden and G. R. Satchler, Nucl. Phys. 84, 177 (1966).

[5]G. Igo, Phys. Rev. Letters 1, 72 (1958); Phys. Rev. 115, 1665 (1959).

[6]G. R. Satchler, Nucl. Phys. 70, 177 (1965).

[7]H. W. Broek, J. L. Yntema, B. Buck, and G. R. Satchler, Nucl. Phys. 64, 259 (1965).

[8]R. M. Drisko, G. R. Satchler, and R. H. Bassel, Phys. Letters 5, 347 (1963).

[9]D. F. Jackson and C. G. Morgan, Phys. Rev. 175, 1402 (1968).

[10]O. N. Jarvis, B. C. Harvey, D. L. Hendrie, and J. Mahoney, University of California Lawrence Radiation Laboratory Report No. UCRL-17352 (unpublished).

[11]P. Darriulat, G. Igo, H. G. Pugh, J. M. Meriwether, and S. Yamabe, University of California Lawrence Radiation Laboratory Report No. UCRL-11054 (unpublished).

[12]C. B. Fulmer, J. Benveniste, and A. C. Mitchell, Phys. Rev. 165, 1218 (1968).

[13]G. J. Pyle, Williams Laboratory Report No. COO-1265-64, 1968 (unpublished).

[14]D. F. Jackson and V. K. Kembhavi, Phys. Rev. 178, 1626 (1969).

PHYSICAL REVIEW C VOLUME 2, NUMBER 2 AUGUST 1970

Level Structure of ^{50}V†

J. N. Bishop and D. J. Pullen

Department of Physics, University of Pennsylvania, Philadelphia, Pennsylvania 19104

and

B. Rosner

Department of Physics, Technion-Israel Institute of Technology, Haifa, Israel

(Received 10 April 1970)

The reaction ^{49}Ti(^{3}He, d)^{50}V has been studied at 15-MeV incident energy with an over-all energy resolution better than 20 keV full width at half maximum. 54 states were observed in ^{50}V up to 6-MeV excitation, and corresponding deuteron angular distributions were measured in the angular interval 7 to 50°. Spectroscopic information has been extracted for 30 of the stronger or well-isolated transitions by means of a distorted-wave analysis of the differential cross sections. The results are compared with nuclear-model predictions.

I. INTRODUCTION

The present investigation of the ^{49}Ti(^{3}He, d)^{50}V reaction forms part of a systematic study of proton states in the $Z = 23$ nuclei excited by means of the (^{3}He, d) reaction. The results for ^{47}V, ^{49}V, and ^{51}V have already been published.[1-3]

Definite spin and parity assignments are known[4] only for the ground state of ^{50}V. Level energies have been rather well established up to 3.7-MeV excitation from studies of the ^{50}Ti($p, n\gamma$),[5] ^{50}Ti(^{3}He, t),[6] ^{50}V(p, p'),[7] ^{50}V(d, d'),[8] ^{51}V(p, d),[9] and ^{52}Cr(d, α)[7] reactions, but tentative spins and parities have been obtained for very few of them. No previous study of the ^{49}Ti(^{3}He, d) reaction has been reported.

II. EXPERIMENTAL TECHNIQUES AND RESULTS

A self-supporting titanium metal foil, enriched to 76% in ^{49}Ti, was bombarded with 15-MeV ^{3}He^{++}